The Astrophysical Journal, 631:85–100, 2005 September 20

GALAXY MORPHOLOGIES IN THE HUBBLE ULTRA DEEP FIELD: DOMINANCE OF LINEAR STRUCTURES AT THE DETECTION LIMIT

Debra Meloy Elmegreen
Vassar College, Department of Physics and Astronomy, Box 745, Poughkeepsie, NY 12604; elmegreen@vassar.edu

Bruce G. Elmegreen
IBM Research Division, T. J. Watson Research Center, P.O. Box 218, Yorktown Heights, NY 10598; bge@watson.ibm.com

Douglas S. Rubin
Wesleyan University, Department of Astronomy, Middletown, CT 06459; dsrubin@wesleyan.edu

and

Meredith A. Schaffer
Vassar College, Department of Physics and Astronomy, Box 745, Poughkeepsie, NY 12604; meschaffer@vassar.edu
Received 2005 March 12; accepted 2005 May 26

ABSTRACT

Galaxies in the Hubble Ultra Deep Field (UDF) larger than 10 pixels (0.″3) have been classified according to morphology, and their photometric properties are presented. There are 269 spiral, 100 elliptical, 114 chain, 126 double-clump, 97 tadpole, and 178 clump-cluster galaxies. We also cataloged 30 *B*-band and 13 *V*-band dropouts and calculated their star formation rates. Chains, doubles, and tadpoles dominate the other types at faint magnitudes. The fraction of obvious bars among spirals is ∼10%, a factor of 2–3 lower than in other deep surveys. The distribution function of axial ratios for elliptical galaxies is similar to that seen locally, suggesting that ellipticals relaxed quickly to a standardized shape. The distribution of axial ratios for spiral galaxies is significantly different than locally, having a clear peak at ∼0.55 instead of a nearly flat distribution. The falloff at small axial ratio occurs at a higher value than locally, indicating thicker disks by a factor of ∼2. The falloff at high axial ratio could be from intrinsic triaxial shapes or selection effects. Inclined disks should be more highly sampled than face-on disks near the surface brightness limit of a survey. Simple models and data distributions demonstrate these effects. The decreased numbers of obvious spiral galaxies at high redshifts could be partly the result of surface brightness selection.

Subject headings: galaxies: evolution — galaxies: formation — galaxies: high-redshift — galaxies: structure

Online material: color figures

1. INTRODUCTION

Galaxies with unusual morphologies appear at high redshift in the Hubble Deep Fields North (Williams et al. 1996) and South (Volonteri et al. 2000), the Hawaiian Deep Field (Cowie et al. 1995), the Tadpole Galaxy field (Tran et al. 2003), the GOODS field (Giavalisco et al. 2004), and the Hubble Ultra Deep Field. Some are recognizable as elliptical and spiral galaxies, but many at $z \geq 1.5$ have more clumpy and irregular structures (e.g., Abraham et al. 1996a, 1996b; Conselice 2005). Chain galaxies, for example, are nearly straight alignments of a half-dozen clumps (Cowie et al. 1995; van den Bergh et al. 1996; Elmegreen et al. 2004c, hereafter Paper I). Tadpole galaxies are curved thin structures with a big clump near one end (van den Bergh et al. 1996; Paper I; Straughn et al. 2004). Luminous diffuse objects are oval distributions of clumpy emission resembling disks (Reshetnikov et al. 2003; Conselice et al. 2004); a subcategory of these, having no bulges or exponential disk light profiles, has been called "clump clusters" (Elmegreen et al. 2004a, hereafter Paper II). Double-clump galaxies have two big clumps. Most of these types are not present in the modern universe, although some probably evolve into normal Hubble types. Characteristic of all the irregular types are enormous clumps of star formation, ∼100 times more massive than the largest star complexes in today's spiral galaxies, as well as thick disks and extreme asymmetries that are most likely the result of interactions and merging.

Here we present morphological data on 884 galaxies in the Hubble Ultra Deep Field (UDF). Magnitudes, colors, and axial ratios of the galaxies are studied.

2. DATA

UDF images were obtained with the *Hubble Space Telescope* Advanced Camera for Surveys (*HST* ACS) by S. Beckwith and coworkers in 2004 and are available on the Space Telescope Science Institute (STScI) archive. The images are 10,500 × 10,500 pixels with a scale of 0.″03 pixel^{-1} (315″ × 315″) in four filters: F435W (*B* band, hereafter B_{435}; 134,880 s exposure), F606W (*V* band, V_{606}; 135,320 s), F775W (*i* band, i_{775}; 347,110 s), and F850LP (*z* band, z_{850}; 346,620 s).

We used the i_{775} image, the deepest of the four images, to search by eye to identify and study galaxies that have major axes larger than 10 pixels (corresponding to 0.″3). The whole UDF field was subdivided into 50 fields of 800 × 800 pixels for identification of objects. Each of these subfields was further subdivided and displayed in IRAF in 100 × 100 pixel increments, which were scanned by eye to search for objects larger than 10 pixels (confirmed by measuring with contour plots out to the 2 σ limit). Our full sample includes 884 galaxies. Morphological classifications were made based on the i_{775} images and aided by contour plots and radial profiles. The galaxies were divided into six categories: chain (114 total), clump cluster (178), double (126),

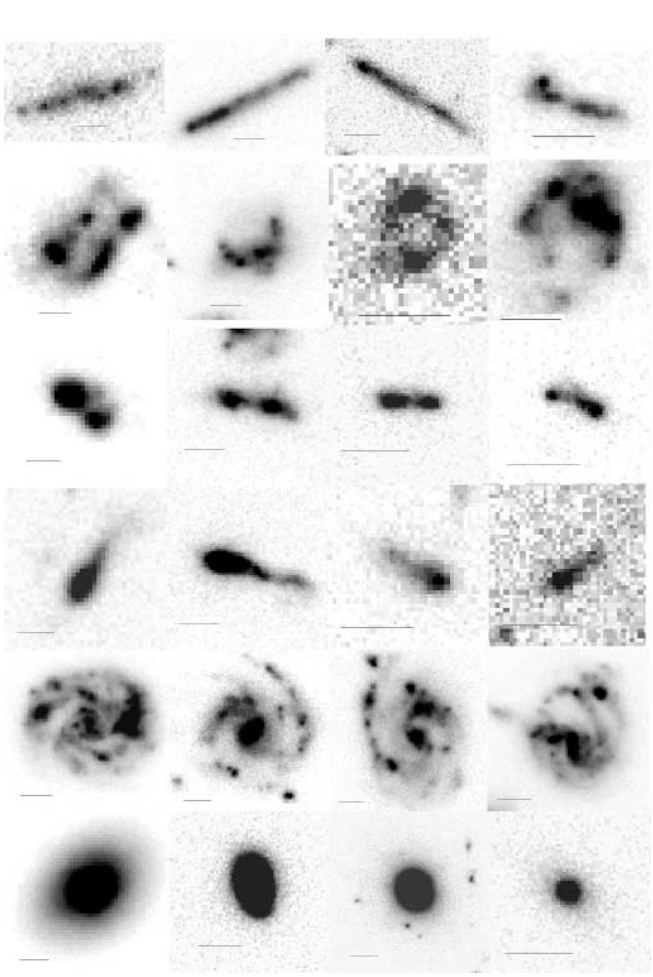

Fig. 1*a*

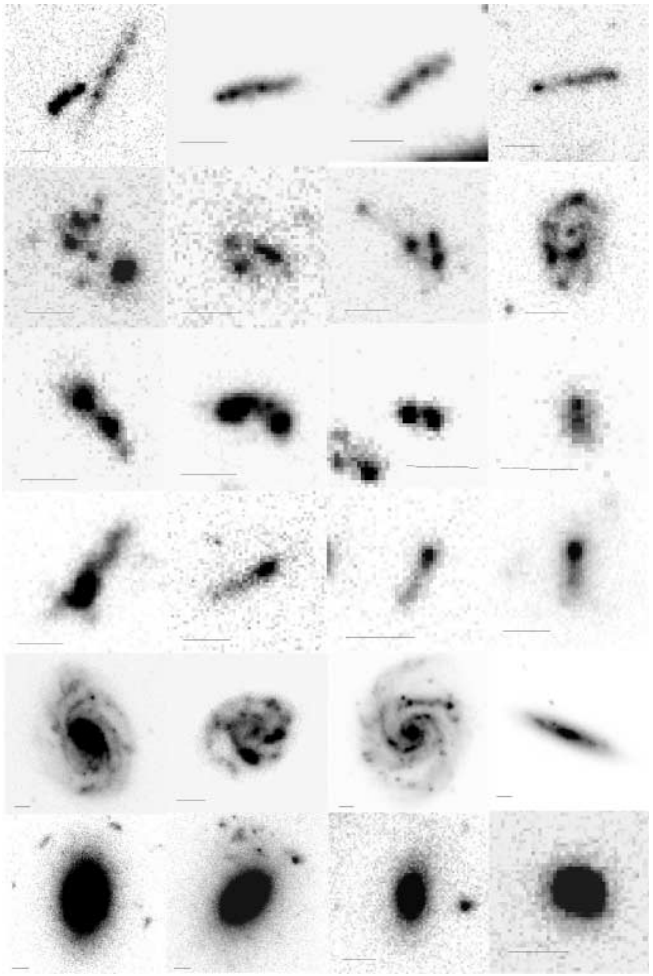

Fig. 1*b*

Fig. 1.—Selection of eight typical galaxies for each morphological type: four in (*a*) and four in (*b*). *Top to bottom*: Chain, clump-cluster, double, tadpole, spiral, and elliptical galaxies. Images are at i_{775} band, with a line representing 0.″5. UDF or our own identification numbers from left to right in (*a*) are as follows: chains: 6478, 7269, 6922, 3214; clump clusters: CC12, 1375, 2291, 5190; doubles: 637, 4072, 5098, 5251; tadpoles: 3058, 8614, 5358, 6891; spirals: 3372, 3180, 4438, 8275; ellipticals: 2107, 4389, 2322, 4913. In (*b*), the identifications are: chains: 169 and 170 (two separate galaxies), 1428, 401, 3458+3418; clump clusters: 6486, 4807, 7230, 9159; doubles: 2461, 2558, 4097, 3967; tadpoles: 9543, 5115, 3147, 9348; spirals: 2607, 5805, 7556, 5670; ellipticals: 8, 4527, 4320, 5959. Panel *b* has an example of an edge-on spiral.

tadpole (97), spiral (269), and elliptical (100). Figure 1 shows eight examples of each type; the lines correspond to 0.″5.

Galaxy morphology can vary with wavelength, so we viewed many of the cataloged objects at other ACS passbands and with NICMOS (Thompson et al. 2005). Generally, the morphological classification does not change significantly with wavelength (e.g., Dickinson 2000) because it is based on only the most fundamental galaxy characteristics, such as elongation and number of giant clumps. Also, the NICMOS images have a factor of 3 lower resolution, so they do not reveal the same fine structure as the other images.

The distinguishing characteristics of the main types that we classified are as follows:

Chain.—Linear objects dominated by several giant clumps and having no exponential light profiles or central red bulges.

Clump cluster.—Oval or circular objects resembling chain galaxies in their dominance by several giant clumps and having no exponential profiles or bulges.

Double clump.—Systems dominated by two similar clumps with no exponential profile or bulge.

Tadpole.—Systems dominated by a single clump that is off-center from, or at the end of, a more diffuse linear emission.

Spiral.—Galaxies with exponential-like disks, evident spiral structure if they have low inclination, and usually a bulge or a nucleus. Edge-on spirals have relatively flat emission from a midplane, and often extended emission perpendicular to the midplane, as well as a bulge.

Elliptical.—Centrally concentrated oval galaxies with no obvious spiral structure.

Chain galaxies were first recognized by Cowie et al. (1995) using the same definition as that here. Tadpole galaxies were defined by van den Bergh et al. (1996), and examples from the UDF were discussed by Straughn et al. (2004). Tadpole galaxies with short tails were classified as "comma" type in the morphology review by van den Bergh (2002). Van den Bergh et al. (1996) also noted objects like clump clusters and called them "protospirals." Conselice et al. (2004) called these clump-dominated young disk galaxies "luminous diffuse objects," although some of their sample included galaxies with bulges and exponential-like profiles, unlike the clump clusters here. Binary galaxies, like our doubles,

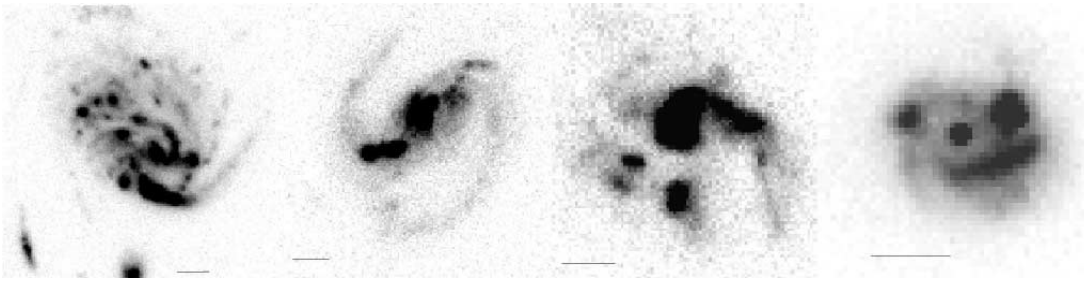

FIG. 2.—Four spiral galaxies showing giant star formation regions, tidal arms, and other asymmetries suggesting interactions. UDF numbers are (*left to right*) 8585, 2, 2993, 7112. UDF 2 has a bar.

were noted by van den Bergh (2002). Other classifications of galaxies in deep *HST* images, based on the Hubble classification or DDO systems, were made by Brinchmann et al. (1998), van den Bergh et al. (2000), and others, who generally noted that an increasing fraction of distant objects fall outside these conventional morphologies.

Distinctions between morphological types do not necessarily imply there are significant physical differences. For example, double-clump galaxies may be smaller versions of chain galaxies, and the single-clump tadpoles may be smaller yet. The origins of these types are not known. Also, chain galaxies and clump clusters may be the same type of object viewed at different orientations (Dalcanton & Schectman 1996; O'Neil et al. 2000; Paper II).

Spiral galaxies are extremely varied. Many look highly disturbed, as if by interactions with smaller companions. Figure 2 shows four more examples of spirals. The galaxy on the left is very asymmetric and has a giant star formation region along the bottom arm. The galaxy on the right is dominated by two round clumps and an extended bright arm (''the cigar smoker'').

Images of 10 different clump clusters from the UDF are in Elmegreen & Elmegreen (2005, hereafter Paper III), where their clump properties were measured. Images of eight different UDF ellipticals are in Elmegreen et al. (2005, hereafter Paper IV), which concentrated on those having giant blue clumps in their centers (one of the ellipticals shown in Fig. 1, UDF 4389, has blue clumps in its core, but they cannot be seen in this image).

Ellipse fits were done on all of the spirals using IRAF to search for radial variations in position angle and ellipticity. Bars have a characteristic signature on such a plot as a result of the twisting inner isophotes. The images were also viewed directly to look for bars. In general, the most highly inclined galaxies do not readily show bars even if they are present, and the short type of bar that is commonly found in local late-type galaxies could not be resolved. Nevertheless, we found 26 barred spirals out of 269 spiral galaxies, a bar fraction of ~10%. This is a factor of ~2 smaller than in the Tadpole field, considering even the inclination effects (Elmegreen et al. 2004b, hereafter Paper V), and it is a factor of ~3 smaller than in the GOODS field (Jogee et al. 2004). The Tadpole field contained 43 barred galaxies in a sample of 186 spirals and showed clear correlations between apparent bar fraction and both inclination and galaxy angular size. The GOODS field contained 80 bars out of 258 nearly face-on spirals. Both previous studies used radial profiles of ellipticity and position angle to identify bars, as we do here. Deeper fields such as the UDF might be expected to show fewer bars as physical resolution and surface brightness dimming become more of a problem at high redshift. Bar destruction by severe interactions (Athanassoula & Bosma 2003) could play a role at high z too. A more thorough study of the UDF bars will be addressed in another paper. Early searches for barred galaxies found relatively few examples (e.g., van den Bergh et al. 2002), probably because of the lower angular resolution of the WFPC2 camera. Sheth et al. (2003) was the first to suggest that the relative numbers of bars might be the same as that found locally.

Two examples of barred spirals in the UDF are shown in Figure 3, along with the radial profiles of ellipticity and position angle. They are the galaxies UDF 1971 (*left*) and UDF 9341. The bars and spirals are more irregular than in local galaxies, suggesting chaotic stellar orbits and poorly defined resonances. The bars could therefore be young. Star formation is enhanced in many small clusters near the top end of the bar in UGC 1971.

The distribution functions of the colors and magnitudes of the clumps that have been measured in chains, clump clusters, doubles, and tadpoles are all about the same (Paper I). Similar also are the colors and magnitudes of clumps in the cores of 30 ellipticals in the UDF (Paper IV). These colors and magnitudes give clump masses in the range from $10^6\,M_\odot$ for the smallest ellipticals (Paper IV) to $10^9\,M_\odot$ for the best studied clump clusters (Paper III), based on stellar population models from Bruzual & Charlot (2003). The clumps are clearly smaller and bluer than the bulges of spiral galaxies (Paper I). The irregular morphology

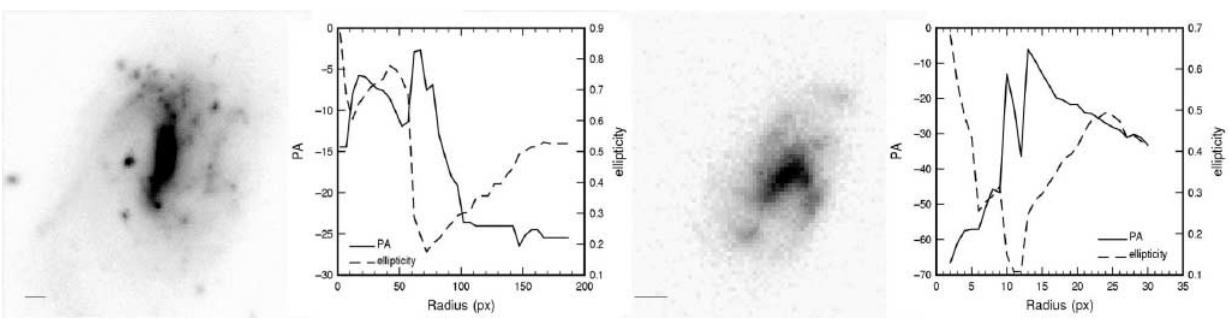

FIG. 3.—Barred spirals UDF 1971 (*left*) and UDF 9341 are shown with their radial distributions of position angle and ellipticity.

TABLE 1
CHAIN GALAXIES

UDF									
65	98	133	169	170	173	401	412	521	666
1236	1287	1383	1428	1531	1678	2034	2265	2394	2426
2750	2763	2764	2998	3001	3091	3143	3214	3299	3354
3368	3459	3529	3607	3693	3779	3974	3977	4010	4013
4243	4387	4411	4568	4581	4660	4674	5010	5014	5053
5225	5380	5454	5497	5787	6017	6278	6391	6450	6478
6523	6539	6607	6634	6709	6715	6922	6941	7037	7076
7269	7352	7617	7681	7737	7816	7868	8092	8097	8268
8372	8624	8681	8731	8801	8805	9171	9270	9414	9676
9839	9861	9974	...	...	...	...	...	...	...

UDF					μ_i	i	$B-V$	$V-i$	$i-z$
1309+1347	...	...	...	...	24.29	23.85	0.55	0.71	0.45
1419+1396	...	...	...	...	25.20	25.77	0.61	0.05	−0.02
2436+2484	...	...	...	...	24.73	25.74	0.38	0.02	0.01
3178+3194	...	...	...	...	25.88	26.09	0.23	0.09	0.08
3458+3418	...	...	...	...	25.07	26.04	2.82	0.63	0.08
4976+4981	...	...	...	...	24.47	24.21	0.04	0.05	0.29
8330+8369+46	...	...	...	...	25.46	24.96	0.80	0.06	−0.08
9085+8865	...	...	...	...	24.61	26.37	1.99	0.47	0.04
9934+...[a]	...	...	...	...	25.06	25.93	0.09	0.46	0.21

Number	x	y	R.A. (J2000.0)	Decl. (J2000.0)	μ_i	i	$B-V$	$V-i$	$i-z$
C1	3081.5	3433	3 32 43.9064	−27 48 23.598	24.32	24.79	0.21	−0.09	0.02
C2	6901.5	2194.5	3 32 35.2695	−27 49 00.793	24.47	25.55	0.88	0.24	0.10
C3	5088	1935	3 32 39.3706	−27 49 08.563	24.60	26.64	2.26	0.76	0.46
C4	1602.4	4288.1	3 32 47.2496	−27 47 57.921	24.79	26.03	1.49	0.30	−0.04
C5	2294.5	7179	3 32 45.6812	−27 46 31.206	24.83	26.68	−0.01	0.05	0.49
C6	7719	2828.5	3 32 33.4207	−27 48 41.777	24.87	24.29	0.28	0.62	0.27
C7	5270	5057.5	3 32 38.9568	−27 47 34.890	25.02	26.71	1.90	0.28	−0.12
C8	4276	8312.5	3 32 41.2011	−27 45 57.229	25.03	28.40	1.13	0.36	0.038
C9	6147	5311.5	3 32 36.9739	−27 47 27.278	25.11	26.47	1.23	1.11	0.65
C10	5076.4	9884.9	3 32 39.3908	−27 45 10.066	25.24	25.79	−0.16	0.43	0.27
C11	5981.5	2948.5	3 32 37.3495	−27 48 38.166	25.26	27.34	0.16	0.09	0.04
C12	5966	2989	3 32 37.3845	−27 48 36.951	25.36	27.60	0.01	0.17	0.21

NOTE.—Units of right ascension are hours, minutes, and seconds, and units of declination are degrees, arcminutes, and arcseconds.
[a] UDF 9934 also includes UDF 9912 and UDF 9949.

of the first four types suggests a history dominated by galaxy interactions, clump accretions, and large-scale instabilities leading to star formation. The highly clumpy structure of the elliptical galaxies suggests a similar history of clump accretions.

Most of the galaxies in this catalog are also listed in the UDF catalog without morphological classifications.[1] Some of the galaxies here are not listed in the UDF catalog because they appear near bright stars or near the edge of the field of view. The parameters used for SExtractor were chosen to optimize different aspects of the UDF than our morphological system, so there is not a one-to-one correspondence. Our catalog has 9 chain galaxies, 14 clump-cluster galaxies, 10 double galaxies, and 1 tadpole galaxy with multiple UDF numbers, and there are 12 chains, 16 clump clusters, 11 doubles, 8 tadpoles, 28 spirals, and 6 ellipticals that are not in the UDF catalog at all. One object, UDF 5898, is two separate spiral galaxies that SExtractor called one, using the midpoint as a position; we call these UDF 5898A and UDF 5898B. The unlisted and multiply-listed galaxies amount to 154 objects, or 17% of the total sample.

[1] The UDF catalog is available on the STScI Web site at ftp://archive.stsci.edu/pub/hlsp/udf/acs-wfc/h_udf_wfc_V1_i_cat.txt.

The integrated AB magnitudes were measured in all four filters from counts within a rectangular box whose edges were defined by the i_{775} isophotal contours 2 σ above the sky noise (corresponding to a surface brightness of 26.0 mag arcsec^{-2}). The integrated magnitudes depend only weakly on the choice of outer isophotal contour: 10 pixel extensions changed the magnitudes of isolated objects by less than 0.1 mag. The integrated $i_{775} - z_{850}$ colors of the galaxies range from −0.7 to 1.3. The integrated i_{775} magnitudes range from 18.5 to 29 mag, with surface brightnesses from 22.5 to 27 mag arcsec^{-2}. The details of some clump properties are given in separate studies of different subsamples (Papers III and IV).

Tables 1–6 list the galaxies by morphological type. In the first part of each table, the galaxies with a single UDF number are listed. In the second part, galaxies with multiple UDF numbers are given along with the combined average surface brightnesses in i_{775}, μ_i, the apparent magnitudes, i, and the three colors. In the third part, galaxies with no UDF numbers are given along with the coordinates of their centers and other properties. We do not repeat the colors and magnitudes of the single sources because these measurements are in the UDF catalog; they are the same as what we measured independently to within 0.1 mag

TABLE 2

CLUMP-CLUSTER GALAXIES

UDF									
40	84	97	126	168	187	533	551	566	769
791	797	853	857	918	941	1041	1112	1266	1269
1316	1362	1375	1589	1666	1681	1693	1775	1859	2012
2174	2240	2291	2340	2350	2350	2463	2499	2538	2853
3021	3031	3037	3154	3243	3270	3460	3483	3688	3689
3745	3752	3778	3799	3844	3877	3881	4006	4084	4093
4094	4253	4262	4370	4616	4807	4860	4999	5050	5107
5136	5190	5201	5216	5491	5501	5548	5579	5620	5634
5683	5685	5748	5827	5837	5860	5878	5896	5946	6056
6133	6187	6394	6396	6438	6456	6486	6499	6645	6710
6785	6821	6837	6854	6939	6943	7185	7227	7230	7328
7432	7526	7559	7647	7678	7725	7756	7786	7905	7995
8022	8042	8125	8217	8262	8270	8314	8461	8551	8682
8710	8749	8765	8802	8859	8880	9000	9112	9159	9273
9299	9347	9356	9396	9409	9474	9837	9853	...	...

UDF					μ_i	i	$B-V$	$V-i$	$i-z$
82+99+103	...	...	...	...	25.07	23.59	0.43	0.25	0.30
3034+3129	...	...	...	...	24.6	24.03	0.82	0.18	0.08
3465+3597	...	...	...	...	24.32	23.48	0.11	0.04	0.02
4245+...[a]	...	...	...	...	26.16	25.08	0.08	0.25	0.32
4258+4458	...	...	...	...	25.12	25.56	0.60	0.27	0.10
4765+4795	...	...	...	...	24.81	25.56	2.03	0.38	−0.01
4801+5271	...	...	...	...	25.17	23.87	0.22	0.37	0.56
6235+6153	...	...	...	...	25.14	25.59	0.01	0.17	0.33
6462+6886	...	...	...	...	25.51	23.48	0.18	0.32	0.27
6713+6738	...	...	...	...	25.24	26.35	3.86	0.62	−0.08
7008+7045	...	...	...	...	25.35	26.16	1.31	0.32	0.08
7081+...[a]	...	...	...	...	25.86	24.52	0.06	0.105	0.34
9169+9332	...	...	...	...	24.88	24.48	0.16	0.18	0.30
9166+9102	...	...	...	...	25.13	24.35	0.32	0.63	0.62

Number	x	y	R.A. (J2000.0)	Decl. (J2000.0)	μ_i	i	$B-V$	$V-i$	$i-z$
CC1	4446	1030	3 32 40.8232	−27 49 35.706	24.32	24.11	1.20	0.24	0.05
CC2	3809.2	1717.2	3 32 42.2627	−27 49 15.082	25.16	24.52	0.88	0.12	0.21
CC3	6154.5	2458	3 32 36.9586	−27 48 52.883	25.14	25.90	0.056	0.45	0.09
CC4	688	5339	3 32 49.3154	−27 47 26.377	23.86	22.00	0.44	0.16	−0.07
CC5	769.3	4832.3	3 32 49.1323	−27 47 41.579	25.36	25.23	0.02	0.26	0.08
CC6	1117	5932.5	3 32 48.3447	−27 47 08.580	25.13	26.14	0.81	0.04	−0.21
CC7	1168.7	6154.3	3 32 48.2275	−27 47 01.927	24.82	26.47	0.49	0.04	−0.18
CC8	8296.5	6395	3 32 32.1142	−27 46 54.784	24.15	25.13	0.99	0.24	0.03
CC9	9018	6086	3 32 30.4832	−27 47 04.055	24.69	26.20	0.17	0.04	0.02
CC10	8824	6572	3 32 30.9217	−27 46 49.475	24.62	24.18	0.75	0.87	0.72
CC11	3702.4	8496.8	3 32 42.4974	−27 45 51.693	23.63	24.38	1.73	0.30	−0.03
CC12	4211.6	8945.3	3 32 41.3461	−27 45 38.245	24.07	23.49	0.37	0.60	0.43
CC13	4256.1	9120.8	3 32 41.2453	−27 45 32.980	24.83	24.30	0.02	0.10	0.07
CC14	4385.7	9269.3	3 32 40.9523	−27 45 28.527	24.03	23.17	0.40	0.60	0.08
CC15	4982	9541	3 32 39.6044	−27 45 20.382	24.53	23.68	0.03	0.44	0.22
CC16	6058.3	9293.7	3 32 37.1721	−27 45 27.811	25.36	26.53	2.32	0.85	0.09

NOTE.—Units of right ascension are hours, minutes, and seconds, and units of declination are degrees, arcminutes, and arcseconds.

[a] UDF 4245 also includes UDF numbers 4450, 4466, 4501, and 4595. UDF 7081 also includes UDF 7136 and UDF 7170.

TABLE 3
Double Galaxies

UDF									
86	178	207	209	475	637	966	985	1000	1416
1619	1662	1667	1796	1955	1992	2032	2215	2461	2558
2943	2954	3248	3351	3373	3454	3513	3527	3701	3895
3907	3933	3967	4040	4072	4082	4097	4137	4228	4313
4461	4479	4569	4581	4603	4644	4685	4686	4699	5098
5159	5251	5304	5405	5456	5574	5632	5669	5784	5788
5928	5956	5962	5964	5983	6128	6137	6139	6209	6254
6411	6487	6543	6681	6754	6808	6957	7159	7234	7318
7622	7711	7815	7907	8207	8273	8326	8327	8419	8637
8664	8878	9024	9092	9110	9139	9304	9308	9330	9406
9414	9505	9706	9720	9777	...	...	...	...	...

UDF					μ_i	i	$B-V$	$V-i$	$i-z$
1829+1752	...	...	...	...	23.42	24.52	0.03	0.20	0.45
2061+2015	...	...	...	...	23.95	27.65	−0.09	0.13	0.32
2130+2156	...	...	...	...	25.01	26.56	0.00	−0.18	−0.11
3377+3398	...	...	...	...	25.85	27.69	0.86	5.27	1.14
5326+5312	...	...	...	...	25.21	27.52	0.11	−0.09	−0.21
5339+5322	...	...	...	...	25.80	26.83	0.91	0.12	−0.12
6356+6351	...	...	...	...	25.24	27.34	0.35	−0.05	−0.09
7694+7702	...	...	...	...	24.82	25.17	1.51	0.37	−0.01
7812+7934	...	...	...	...	26.08	27.25	0.93	0.29	−0.02
8966+9011	...	...	...	...	24.70	25.12	0.74	0.20	0.11

Number	x	y	R.A. (J2000.0)	Decl. (J2000.0)	μ_i	i	$B-V$	$V-i$	$i-z$
D1	7302.1	2360.1	3 32 34.3636	−27 48 55.827	23.17	24.76	3.05	0.92	0.14
D2	7409.8	2568.1	3 32 34.1200	−27 48 49.588	24.01	23.92	0.29	0.08	0.01
D3	606.9	5159.6	3 32 49.4990	−27 47 31.757	24.78	25.82	0.96	0.26	−0.18
D4	1760.7	6704.9	3 32 46.8884	−27 46 45.420	24.22	25.57	0.50	−0.07	−0.15
D5	6490.2	7924.1	3 32 36.1967	−27 46 08.902	24.65	25.65	0.34	0.13	−0.02
D6	8126.9	7044.6	3 32 32.4974	−27 46 35.295	24.80	26.98	0.97	0.40	−0.09
D7	8730.4	6496.7	3 32 31.1333	−27 46 51.734	24.97	26.74	0.17	−0.00	−0.16
D8	4036.3	8687.9	3 32 41.7425	−27 45 45.965	24.84	26.11	0.50	0.08	−0.01
D9	4696.6	564.7	3 32 40.2569	−27 49 49.668	24.21	25.19	0.53	0.38	0.32
D10	5211.6	683.6	3 32 39.0920	−27 49 46.107	24.70	25.81	0.36	0.21	0.15
D11	1094.8	6186.3	3 32 48.3945	−27 47 00.966	24.86	27.70	0.88	2.43	−0.05

Note.—Units of right ascension are hours, minutes, and seconds, and units of declination are degrees, arcminutes, and arcseconds.

(which is the same as the measuring error for UDF magnitudes). Barred galaxies are indicated with an asterisk in the spiral list.

3. PHOTOMETRIC RESULTS

The average color and magnitude values for each galaxy type are shown in Figure 4. This plot has more observational relevance than physical because the galaxies are a mixture of redshifts and k-corrections. The average i_{775} surface brightness is fairly constant at $\sim$24.8 mag arcsec^{-2} for all types except ellipticals, which are about 0.5 mag brighter. This constancy is likely the result of the surface brightness limit of the survey (2 σ is 26.0 mag arcsec^{-2}), with the averages being larger than this limit because of central light concentration. The average i_{775} integrated magnitude is about 26.3 for chains, doubles, and tadpoles, 24.5 for spirals, 24.2 for ellipticals, and 25.2 for clump clusters. The ellipticals have the reddest colors in all indices.

The surface brightness distribution of all the galaxies peaks at $\sim$25 mag arcsec^{-2}, rapidly declines beyond the 2 σ limit of 26.0 mag arcsec^{-2}, and is virtually null beyond the 3 σ limit of 26.6 mag arcsec^{-2} (see also Fig. 11 below).

Figure 5 plots $B_{435} - V_{606}$ versus $i_{775} - z_{850}$ for all galaxies in our sample, divided according to morphology. Note the Lyman break galaxies of various types, which have extremely red $B_{435}-V_{606}$ colors. Except for these, the color distributions are similar with a large number of galaxies at $B_{435} - V_{606} \sim 0$ and a second diagonal branch going up to $B_{435} - V_{606} \sim 2$. The curves superposed on the data are Bruzual & Charlot (2003) evolution models that assume star formation began at $z = 6$ for all cases and then decayed exponentially over time with e-folding times of 0.01 Gyr, 0.03 Gyr, 0.1 Gyr, 0.3 Gyr, 1 Gyr, 3 Gyr, and infinity. Each curve traces the sequence of decay times with the longest decay times corresponding to the bluest colors. The different curves are for different galaxy redshifts, from 0 to 4 in steps of 0.5 (see color coding in figure caption). The models are described more in Paper III.

The distribution of colors reveals several things about these galaxies. The chains, clump clusters, doubles, and tadpoles have similar color distributions, and the spirals have about the same distribution too, but the spirals do not have the very red $B_{435}-V_{606}$ and $i_{775} - z_{850}$ components that are present in the more irregular systems. These red points correspond to the highest redshifts, $z \sim 4$, so the difference in distribution suggests the spirals do not generally go to as high a redshift as the more irregular and clumpy galaxies. There is a spiral, UDF 7036, that has the colors

TABLE 4
TADPOLE GALAXIES

				UDF					
38	83	110	141	176	197	285	648	719	741
1454	1469	1720	2044	2230	2445	2542	2785	2872	2879
2881	3058	3059	3128	3147	3185	3442	3468	3508	3573
3583	3682	3819	3823	3893	3906	3945	4053	4184	4187
4287	4390	4548	4592	4601	4638	4668	4717	4838	4841
4908	4927	5063	5115	5124	5358	5377	5386	5388	5443
5533	5674	5843	6119	6290	6782	6891	6999	7044	7146
7202	7210	7862	7900	7962	8006	8150	8523	8561	8580
8614	8750	8950	8964	9310	9348	9543	9848	...	...

UDF					μ_i	i	$B-V$	$V-i$	$i-z$
4348+4352	...	...	...	...	26.28	26.34	1.20	0.15	0.36

Number	x	y	R.A. (J2000.0)	Decl. (J2000.0)	μ_i	i	$B-V$	$V-i$	$i-z$
T1	679.05	5958.7	3 32 49.3347	−27 47 07.786	25.11	25.71	0.31	−0.06	−0.07
T2	4170.6	6467.2	3 32 41.4410	−27 46 52.587	24.78	25.17	0.72	0.45	0.25
T3	3557.2	8235.3	3 32 42.8258	−27 45 59.536	24.74	24.13	0.62	0.73	0.19
T4	4290.2	9000.2	3 32 41.1684	−27 45 36.599	24.13	26.04	−0.02	0.56	0.38
T5	3997.1	8840.1	3 32 41.8310	−27 45 41.398	24.47	25.92	−0.02	0.13	0.35
T6	8623.6	3759.6	3 32 31.3751	−27 48 13.847	24.74	26.31	3.11	2.20	0.52
T7	5885.9	1300.1	3 32 37.5667	−27 49 27.618	24.58	25.23	1.72	0.57	0.08
T8	6236.8	1462.7	3 32 36.7730	−27 49 22.742	24.70	24.98	0.24	0.49	0.08

NOTE.—Units of right ascension are hours, minutes, and seconds, and units of declination are degrees, arcminutes, and arcseconds.

of a *B*-band dropout, however, so it could be at $z \sim 4$ (see § 6 and Table 7). Selection effects could remove the most easily recognized spirals, which are the face-on spirals, from our sample (see § 5). The irregular and spiral galaxies both populate the bluer regions in Figure 5, which suggests that both types linger around in cosmological time after the spirals become obvious (see also Franceschini et al. 1998).

The ellipticals also extend in Figure 5 to the high $V_{606} - i_{775}$ and $B_{435} - V_{606}$ values of the clumpy types. The ellipticals are slightly redder than the other types, lacking the big clump of points around $i_{775} - z_{850} \sim 0$ and $B_{435} - V_{606} \sim 0$ that all the others have. Evidently the ellipticals have much less star formation at the epoch of observation, as is well known (e.g., Ferguson et al. 2000).

4. RELATIVE NUMBERS

Figure 6 plots the number and fraction of galaxies of each type as a function of i_{775} magnitude. The counts of galaxies with spiral or elliptical morphologies peak at about the same apparent magnitude, which is slightly brighter than the peak of the clump clusters. The counts of chain, double, and tadpole galaxies all peak at about 1 mag fainter. The fractions follow a similar trend, with spirals dominating the bright galaxies, while chains, doubles, and tadpoles dominate the faint galaxies. As is well known, the galaxies with the most unusual morphologies increase in dominance at the faintest magnitudes, beyond $i_{775} \sim 26$.

The trend for chains, doubles, and tadpoles to dominate at the faintest magnitudes illustrates an important selection effect discussed in the next section. We believe on the basis of this trend, and on the basis of the distribution of axial ratios for spirals, that the spirals begin to disappear at $i_{775} \sim 26$ because the face-on spirals become too faint to see at the surface brightness limit of the survey ($\sim$26.0 mag arcsec^{-2} for 2 σ detections). Edge-on spirals have higher surface brightnesses than face-on spirals and are observed to fainter magnitudes. In the distribution of axial ratios (see below), there is a clear and unusual drop in the count for face-on spirals. In the same way, the chain galaxies extend to fainter magnitudes than the clump clusters in Figure 6 because chain galaxies are probably edge-on clump clusters (Paper II). Edge-on galaxies tend to have higher surface brightnesses and fainter apparent magnitudes than face-on galaxies (see models in Paper I). Thus, the faintest galaxies at the surface brightness limit of detection are observed to be linear structures, many of which are probably flattened objects viewed edge-on. The tadpole galaxies, for example, could be strongly interacting galaxies with a 10^9–$10^{10}\ M_\odot$ merger remnant seen as a single clump at one end and a long tidal tail seen as the diffuse lane (e.g., see Straughn et al. 2004).

5. AXIAL RATIOS

Figure 7 compares the distribution of axial ratios, *W*/*L*, for elliptical galaxies in the UDF field with the distribution for local ellipticals in the *Third Reference Catalogue of Bright Galaxies* (RC3; de Vaucouleurs et al. 1991). The UDF ratios came from the ellipse fits in the published UDF catalog. The error bars equal $N^{1/2}$ for number *N*. For the UDF distribution, the dashed histogram is for the half of the sample with the brightest average surface brightness ($\mu_I < 24.4$ mag arcsec^{-1}). This bright half is slightly rounder on average than the faint half, as observed locally (Tremblay & Merritt 1996). The overall distribution for UDF ellipticals resembles the distribution for local galaxies, particularly for the high surface brightness ellipticals, suggesting that elliptical galaxies relaxed to their current forms at very early times.

The distribution of axial ratios for spiral galaxies is shown in Figure 8. The spiral galaxies in the deep field background of the Tadpole Galaxy (Tran et al. 2003; Paper I) are shown on the top left. The UDF spirals are on the bottom left. We divided the UDF spirals into the faint surface brightness half and the bright surface brightness half and plotted the separate distributions on the right of Figure 8. For the UDF spirals, the solid-line histograms use

TABLE 5

SPIRAL GALAXIES

UDF									
1	2	13	14	15	17	20	37	43	50
55	95	131	163	192	213	235	237	295	328
355	423	424	428	446	501	503	522	542	656
662	679	697	735	833	898	916	968	1006	1049
1052	1057	1270	1403	1421	1426	1478	1551	1571	1592
1612	1626	1668	1732	1739	1789	1809	1830	1889	1898
1904	1905	1922	1971*	2017	2104	2170	2189	2306	2332
2333	2358	2462	2525	2607	2652	2753	2799	2813	2993
3006	3013	3068	3075	3097	3101	3123	3180	3203*	3247
3257	3268	3315	3319	3349*	3372	3422	3445	3472	3492*
3610	3613*	3680	3785	3822*	3823	3840	3871	4052	4058
4192	4225	4315	4321	4360	4394	4407	4410	4438	4478
4491	4591	4661	4662	4767	4816	4835	4878	4907	4929
4950	5022	5177*	5268	5276	5286	5365*	5408	5411	5417
5435	5473	5505	5540	5569	5606*	5614	5615	5658	5670
5694	5697	5753	5805	5812	5864	5898A[a]	5898B[a]	5922	5989
5995	5999	6008	6038	6051*	6060	6079	6082	6107	6143
6188	6203	6206	6639	6674	6680	6810	6834	6862*	6911
6933*	6974	6997*	7022	7036	7067	7071	7112	7203*	7406
7452*	7495	7556	7664	7688*	7705	7743	7775	7847	7974
8015	8026*	8040	8049*	8051	8156	8181	8255	8257	8259
8261	8275	8351	8409	8454	8576	8585	8603	8629	8693
8757	8782	8918	9018*	9074	9125	9183	9204	9253	9341*
9425	9444*	9455	9599	9609	9649	9724	9759	9807	9834
9895	...	...	...	...	...	...	...	...	...

Number	x	y	R.A. (J2000.0)	Decl. (J2000.0)	μ_i	i	$B-V$	$V-i$	$i-z$
s1*	5102.6	538.9	3 32 39.3387	−27 49 50.446	24.54	23.59	0.78	0.61	0.19
s2	6144.9	1292.1	3 32 36.9810	−27 49 27.860	24.50	24.92	0.18	0.59	0.17
s3	6211.3	1497.7	3 32 36.8307	−27 49 21.692	25.29	25.56	0.21	0.71	0.31
s4	2806.1	2886.6	3 32 44.5297	−27 48 39.986	24.17	24.43	0.88	0.28	0.21
s5	3916.9	2413.6	3 32 42.0184	−27 48 54.192	25.35	25.63	1.25	0.92	0.16
s6	5150.1	2557.2	3 32 39.2298	−27 48 49.898	24.73	25.63	0.67	0.09	0.04
s7	7100.9	2372.6	3 32 34.8186	−27 48 55.451	24.55	24.48	0.76	0.20	0.10
s8	7845.6	3062.1	3 32 33.1344	−27 48 34.769	24.82	23.85	0.58	0.65	0.14
s9	1982.1	3846.9	3 32 46.3917	−27 48 11.164	25.58	25.72	0.20	0.01	−0.09
s10	1958.1	3902.1	3 32 46.4459	−27 48 09.507	24.96	25.09	1.14	0.60	0.09
s11	1640.9	4158.1	3 32 47.1627	−27 48 01.822	25.03	25.36	1.05	0.26	−0.01
s12	8265.1	3406.9	3 32 32.1858	−27 48 24.427	25.19	23.60	0.91	0.23	0.18
s13*	9257.4	4315.4	3 32 29.9420	−27 47 57.173	23.96	22.68	1.84	1.21	0.48
s14	9193.8	4319.4	3 32 30.0858	−27 47 57.053	24.77	25.53	0.29	0.11	0.04
s15	1120.9	4920.6	3 32 48.3373	−27 47 38.937	24.95	24.55	0.88	0.17	0.04
s16	846.4	5071.1	3 32 48.9577	−27 47 34.417	24.97	25.34	0.92	0.22	0.04
s17*	9372.6	5878.6	3 32 29.6816	−27 47 10.277	24.32	23.57	1.22	0.99	0.31
s18	9350.6	6065.6	3 32 29.7313	−27 47 04.667	25.01	24.94	1.23	0.42	0.21
s19	5224.5	7207.5	3 32 39.0581	−27 46 30.390	23.57	24.13	0.84	0.31	0.17
s20*	7461.9	7446.6	3 32 34.0005	−27 46 23.233	24.82	23.95	0.54	0.39	0.02
s21	4064.1	8767.1	3 32 41.6796	−27 45 43.589	24.55	24.80	0.78	0.59	0.16
s22	5011.9	9501.1	3 32 39.5369	−27 45 21.580	25.36	24.16	0.02	0.7	0.4
s23	6490.1	9002.3	3 32 36.1963	−27 45 36.556	24.60	22.29	0.98	0.65	0.29
s24	6662.9	8585.6	3 32 35.8060	−27 45 49.058	24.40	22.93	0.30	0.51	0.17
s25	6994.6	8230.3	3 32 35.0564	−27 45 59.719	24.78	23.71	0.13	0.66	0.30
s26*	6431.0	8852.9	3 32 36.3300	−27 45 41.038	24.18	25.10	0.16	0.63	0.28
s27	5736.6	9952.6	3 32 37.8987	−27 45 08.041	23.91	24.38	0.57	0.85	0.49
s28	5623.6	9773.9	3 32 38.1542	−27 45 13.401	23.93	22.19	1.03	1.28	0.48

NOTES.—Units of right ascension are hours, minutes, and seconds, and units of declination are degrees, arcminutes, and arcseconds. Barred galaxies are indicated by an asterisk.

[a] The coordinates of UDF 5898A are $3^{h}32^{m}31\overset{s}{.}3973$, $-27^{\circ}47'13\overset{''}{.}785$; the coordinates of UDF 5898B are $3^{h}32^{m}31\overset{s}{.}3967$, $-27^{\circ}47'13\overset{''}{.}096$.

TABLE 6
Elliptical Galaxies

UDF									
8	25	36	68	97	100	153	176	191	206
221	287	310	582	600	631	703	731	865	900
901	1088	1344	1358	1453	1481	1564	1607	1727	1960
2016	2063	2107	2162	2201	2245	2248	2293	2322	2329
2387	2414	2518	2927	2974	3048	3088	3136	3174	3288
3332	3333	3475	3591	3677	3869	4096	4142	4320	4350
4389	4396	4445	4481	4527	4551	4587	4805	4913	5187
5263	5959	6018	6022	6027	6047	6288	6747	6853	6853
7121	7398	7780	8069	8138	8316	8680	9090	9264	9532
9765	9778	9847	9962	...	...	...	...	...	...

Number	x	y	R.A. (J2000.0)	Decl. (J2000.0)	μ_i	i	$B-V$	$V-i$	$i-z$
E1	4154.8	1231.1	3 32 41.4815	−27 49 28.72	24.92	26.05	0.36	0.62	0.20
E2	6004.4	1086.9	3 32 37.2988	−27 49 34.02	24.75	25.42	0.40	0.62	−0.19
E3	9026.7	4118.9	3 32 30.4637	−27 48 03.07	24.24	23.52	1.15	0.49	0.15
E4	3674.5	8546.7	3 32 42.5604	−27 45 50.20	23.56	22.36	0.28	1.04	0.18
E5	5741.9	9595.4	3 32 37.8870	−27 45 18.76	23.80	23.79	0.35	0.86	0.29
E6	4826.6	9687.6	3 32 39.9555	−27 45 15.98	25.13	25.75	0.60	0.30	0.14

Note.—Units of right ascension are hours, minutes, and seconds, and units of declination are degrees, arcminutes, and arcseconds.

the ellipticities given in the UDF catalog and the dashed-line histograms use ellipticities derived individually for each galaxy from ellipse fits in IRAF. Because the spirals are irregular, we did not want to use the SExtractor ellipticities exclusively. To check the first two ellipticity measures, we also determined the axial ratios ($W/L = 1 -$ ellipticity) by eye, based on the length (L) and width (W) of the average 2 σ contour limits for each galaxy. All three axial ratio determinations correlated well with each other, to within 0.1 in W/L. In what follows we consider only the axial ratios determined by the UDF automatic ellipse fit and by our IRAF ellipse fits, which are more objective than the visual fits to contour shapes.

The distribution of axial ratios for spirals does not resemble the local distributions for spirals, which is reproduced in Figure 9 using data from the RC3. The local distribution is relatively flat from $W/L \sim 1$ down to $W/L \sim 0.1$, depending on Hubble type, indicating that the objects are round disks with intrinsic axial ratios comparable to this lower limit. The only exception is for spirals of de Vaucouleurs type 9, which are Sm irregulars and known to be relatively thick.

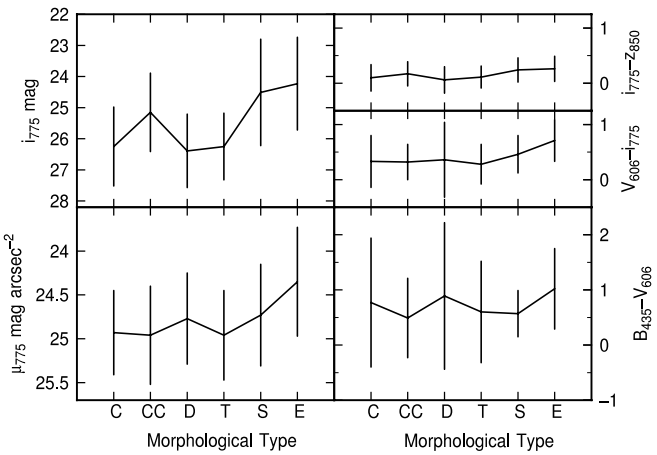

Fig. 4.—Average magnitudes (*top left*), surface brightnesses (*bottom left*), and colors (*right*) are shown for each galaxy type, with 1 σ rms fluctuations from sample varieties. Ellipticals are the reddest and brightest galaxies.

The UDF and Tadpole-field spirals have a distribution of axial ratios that is peaked in the middle, which means that the catalog lacks face-on examples ($W/L \sim 1$). The falloff at low W/L is probably from the intrinsic disk thickness, as for local galaxies, although these spiral disks are evidently ~2 times thicker than the local versions (e.g., Reshetnikov et al. 2002; Papers II and III). The falloff at high W/L could arise if the spirals are intrinsically elongated disks, i.e., not circular, as suggested for local irregular galaxies (Binggeli & Popescu 1995; Sung et al. 1998). Alternatively, they could be circular disks that tend to be overlooked when viewed face-on. We consider these two options in detail now.

Figure 10 shows several models for the projected axial ratios of intrinsically oval, i.e., triaxial, disks. The two on the left show simple cases and the two on the right are sample fits to the UDF or Tadpole data. The model on the bottom left is for circular thick disks with a range of relative thicknesses, $Z/L = 0.225$–0.375, viewed in projection at random angles. The flat part extending to $W/L = 1$ is a result of the circular form of the disk itself, and the rise and fall below $W/L \sim Z/L$ is for the edge-on case, when the minimum axial ratio is viewed. The top left is for an ellipsoid with an axial ratio of 1 : 0.6 : 0.2. The peak at $W/L = 0.6$ is from the main disk axial ratio, when the disk is viewed face-on. The two peaks at $W/L = 0.2$ and 0.33 are for edge-on versions; the lower ratio corresponds to the case where the oval disk is viewed edge-on parallel to the minor axis (showing the major axis length in projection), and the higher ratio corresponds to the case where the oval disk is viewed edge-on along the major axis (showing the minor axis length in projection). Neither of these ideal cases matches the data, but mixtures of them do. The models on the right span a range of intrinsic W/L and Z/L ratios, viewed in projection for orientations of the ellipsoid at random angles in three-dimensional space.

Evidently, the distribution of axial ratios observed for the UDF is consistent with intrinsically elongated spiral disk galaxies. If the disks are actually distorted like this, then tidal forces would be a likely explanation. Such an interpretation is plausible in view of the importance of galaxy interactions at

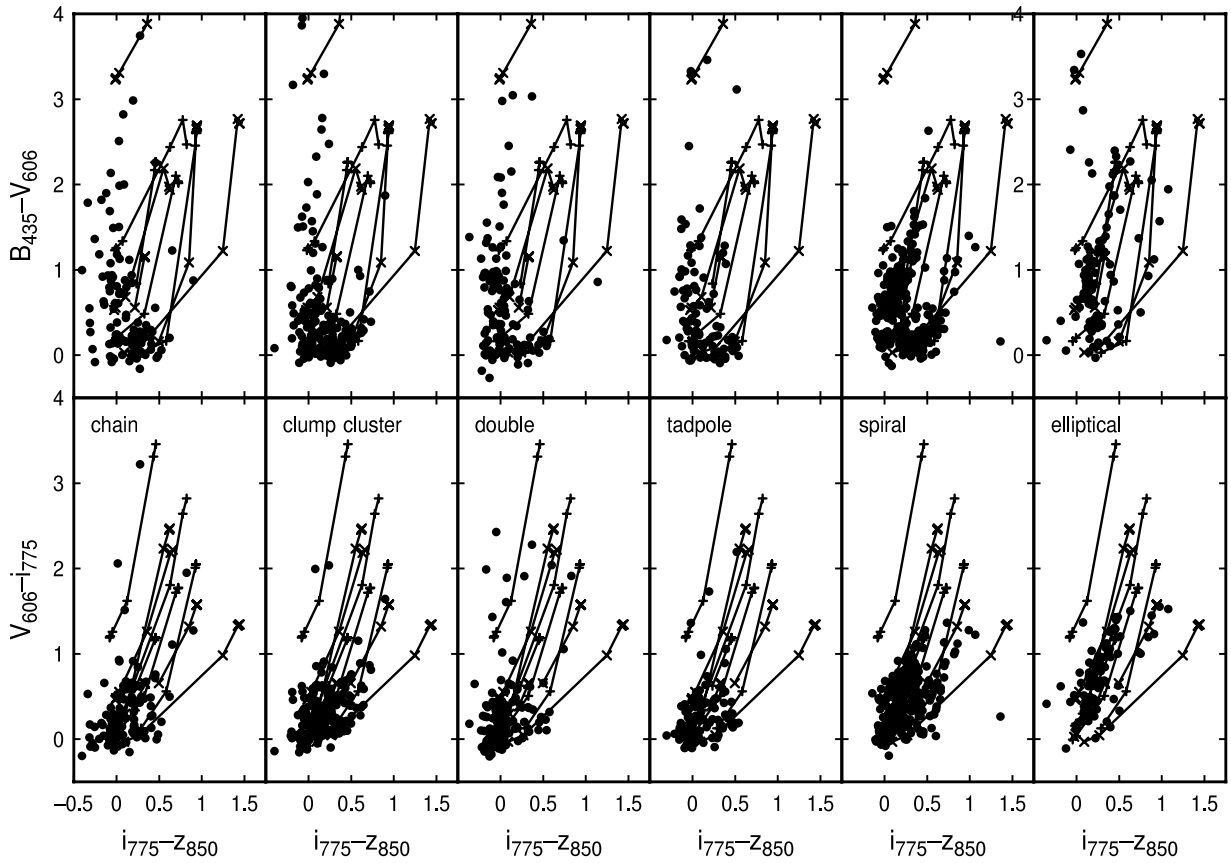

FIG. 5.—Color-color distributions are shown for all 884 galaxies divided by morphology. Superposed curves are stellar evolution models for redshifts 0 (*blue cross*), 0.5 (*blue plus sign*), 1 (*green cross*), 1.5 (*green plus sign*), 2 (*magenta cross*), 2.5 (*magenta plus sign*), 3 (*red cross*), 3.5 (*red plus sign*), 4 (*black cross*), and 4.5 (*black plus sign*). The models assume star formation began at $z = 6$ and decayed exponentially; the curves trace out the colors as the *e*-folding time in Gyr varies as 0.01, 0.03, 0.1, 0.3, 1, 3, and infinity (high decay times are the most blue). [*See the electronic edition of the Journal for a color version of this figure.*]

TABLE 7
LYMAN BREAK DROPOUT GALAXIES

UDF	SFR	UDF	SFR	UDF	SFR
		B-Band Dropouts			
65(C)	7.9	4548(T)	7.7	6808(D)	4.8
141(T)	9.5	4551(E)	16	7036(S)	77
401(C)	21	4685(D)	14	7044(T)	3.1
631(E)	8.4	4765+4795(CC)	21	8092(C)	16
985(D)	5.7	5548(CC)	12	8419(D)	6.6
2394(C)	3.7	6137(D)	2.3	9085+8865(C)	9.7
3001(C)	2.0	6209(D)	1.5	9310(T)	1.8
3458+3418(C)	13	6450(C)	3.8	C7(C)	7.1
3778(CC)	19	6543(D)	15	E19.47(E)	15
4313(D)	4.1	6709(C)	1.1	CC11(CC)	61
		V-Band Dropouts			
1796(D)	6.2	5928(D)	6.5	8326(D)	18
2350(CC)	42	6139(D)	63	8664(D)	23
2881(T)	58	6681(D)	24	8682(CC)	50
3377+3398(D)	30	7328(CC)	465	D11(D)	9.9
5225(C)	48	...	...	...	...

NOTES.—Initials for each morphological type are given as follows: C = chain, CC = clump cluster, D = double, T = tadpole, S = spiral, and E = elliptical. Star formation rates are given in units of $M_{\odot}$ yr^{-1}.

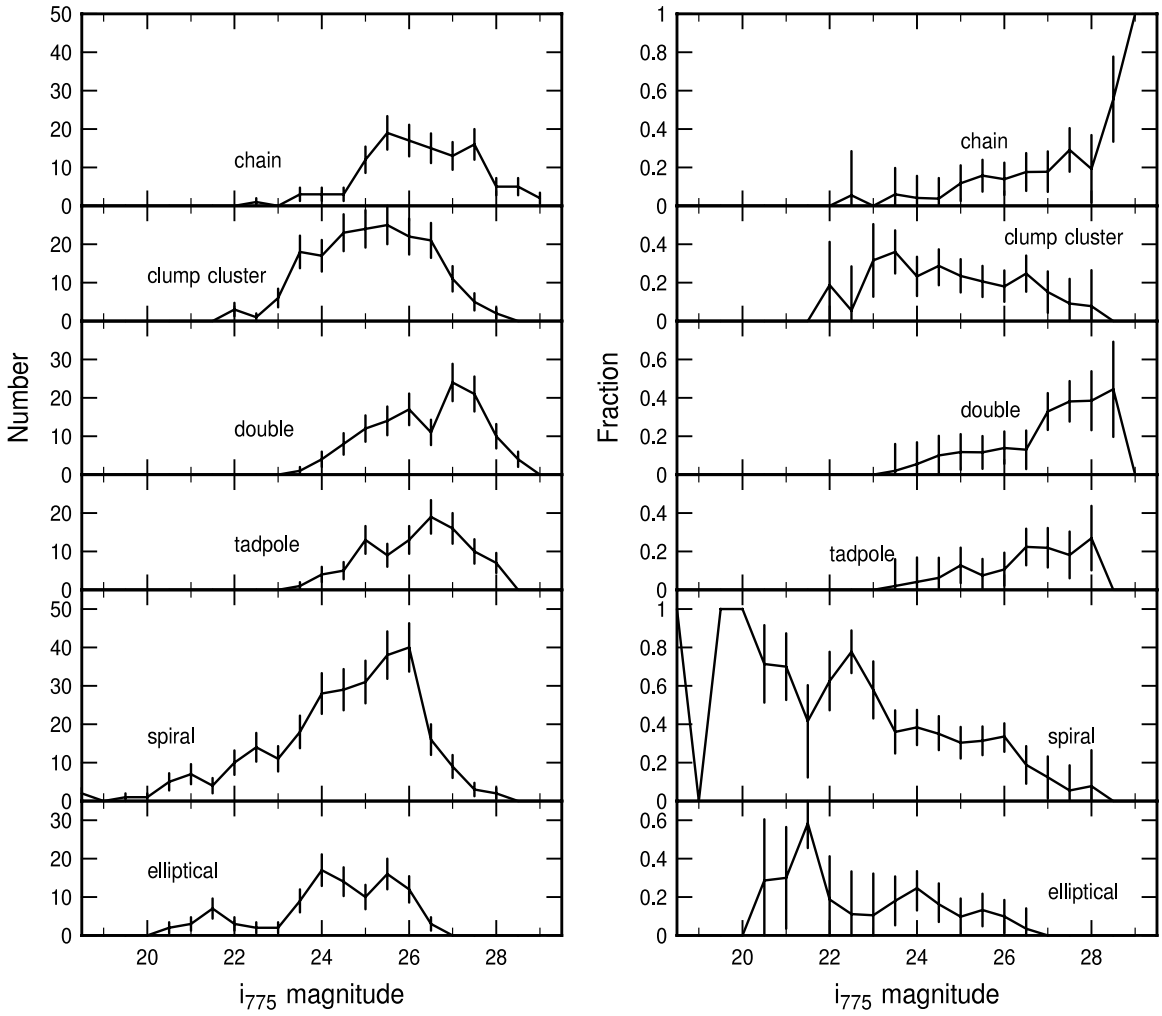

FIG. 6.—Number and fraction of each galaxy type is shown as a function of apparent magnitude, with 1 σ error bars. Linear structures dominate at the faintest magnitudes.

high redshift. However, visual examination of each UDF spiral suggests that very few of the elongated cases have companion galaxies or other direct evidence of a strong interaction. Thus we consider another explanation, as follows.

Recall that Figure 8 showed that the distribution of axial ratios for the low surface brightness spirals is slightly more skewed toward edge-on than the distribution for the high surface brightness spirals. This distortion is shown again in Figure 11, which plots the i_{775} magnitudes and average surface brightnesses (out to the 2 σ contour) versus the axial ratios. The solid red line is the average of the plotted points, which are from the UDF catalog. The dashed red line is the average for the W/L values we measured based on IRAF ellipse fits (these values are not plotted). The density of points on this plot increases for intermediate W/L, reflecting the peak at intermediate W/L in Figure 8. The density of points shifts to even lower W/L at the faintest surface brightnesses (*top part of top panel*), and this shift also parallels the trend in Figure 8.

The bottom panel of Figure 11 shows that the average flux becomes $\sim$2 mag brighter as the spiral galaxies become more face-on. This brightening also occurs for local spirals because the total flux increases as the projected area increases and stars become less obscured by midplane dust.

The top panel of Figure 11 indicates that the average surface brightness is either constant or increases slightly ($\sim$0.5 mag) for more face-on spirals, which is contrary to expectations. Locally the surface brightness decreases for face-on disks because the path length through the stars decreases (Paper I). The situation changes, however, if most of the UDF surface brightnesses for spirals are below the detection limit. This limit is 26 mag arcsec^{-2} for the faintest contour that defines our sample, so the average surface brightness of a typical galaxy inside this contour is greater, perhaps by a magnitude. The two dashed green lines in this figure represent the approximate region where we begin to lose galaxies at the surface brightness limit. Above $\sim$26 mag arcsec^{-2}, the integrated surface brightness would be fainter than the lowest contour considered here (2 σ) and the galaxy would not likely be in our survey. Thus we should ask what a distribution of surface brightnesses should look like if the average surface brightness decreases with increasing W/L as for local galaxies, and as it decreases, the detection limit is passed so the fainter galaxies become lost in the noise. The solid green line shows what the average distribution of surface brightnesses should be if a face-on galaxy is at 25.9 mag arcsec^{-2} (where $W/L = 1$) and edge-on galaxies become brighter in proportion to the path length through the disk (i.e., $\mu = 25.9 - 2.5 \log L/W$). This solid line is well populated with observed galaxies at low W/L so the number of points in the plot is large there, but as W/L increases, the surface brightness limit comes in and the number of points centered on the line decreases.

Another way to see this surface brightness limit is with Figure 6. There we noted that the spiral count (*left panel*) drops

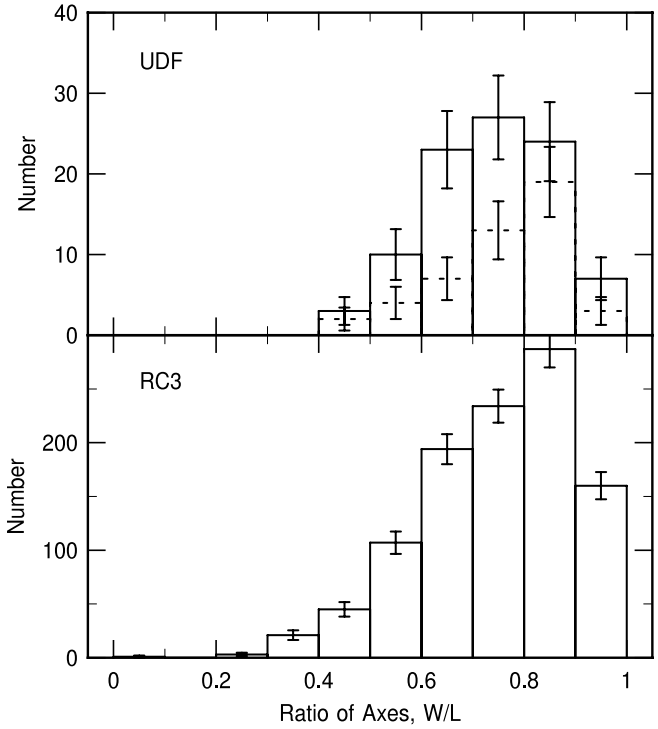

FIG. 7.—Distribution of the ratio of axis for elliptical galaxies in the UDF compared to the RC3. The dotted histogram for the UDF is for the half with the highest surface brightness. The UDF distribution resembles the local distribution, suggesting that elliptical galaxy shapes are standard and were probably determined relatively quickly in the early universe.

precipitously for galaxies fainter than $i_{775} \sim 25.5$ mag, which is about where the distributions of chains, doubles, and tadpoles—all linear systems—begin to peak. This drop may be combined with a model result in Paper I to explain the factor of 5 drop in the axial ratio distribution function between $W/L = 0.5$ and 1 (Fig. 8). Paper I showed in its Figure 8 a radiative transfer model through a thick exponential disk with various levels of extinction; the average disk surface brightness of the projected disk was plotted versus the axial ratio. As W/L increased from 0.5 to 1, the average surface brightness decreased by factors of 1.92, 1.78, and 1.74 for perpendicular extinctions to the midplane at the galaxy center equal to 0.33, 1.33, and 1.77 optical depths. The limiting case with no extinction would be a factor of 2, which is the inverse ratio of the two W/L values, as this intensity ratio is mostly the ratio of path lengths along the line of sight. For these three extinctions, the surface brightness dimming in going from $W/L = 0.5$ to 1 corresponds to 0.71, 0.63, and 0.61 mag arcsec^{-2}. Such magnitude changes correspond, in Figure 6, to more than half of the full drop in spiral galaxy counts (*left panel*). This means that at the limit of the UDF survey, projection effects alone can change a galaxy that would be detected at $W/L < 0.5$ to one that would be below the limit of detection at $W/L \sim 1$.

A simple model for the probability of detection of disk galaxies near the surface brightness limit of a survey is shown in Figure 12. This model assumes that the intrinsic surface brightness distribution of face-on spiral galaxies, in magnitudes per arcsecond, is Gaussian, i.e., that the distribution of intensity is lognormal. This assumption is consistent with the narrow range of surface brightnesses for modern spiral galaxies (Freeman 1970) and with the Tully & Fisher (1977) relation, which suggests the same narrow range. In terms of the model in the top panel of Figure 11, the breadth of the Gaussian would give the intrinsic vertical range of points around the solid green line. For Figure 12, we integrate over this lognormal distribution to find the relative

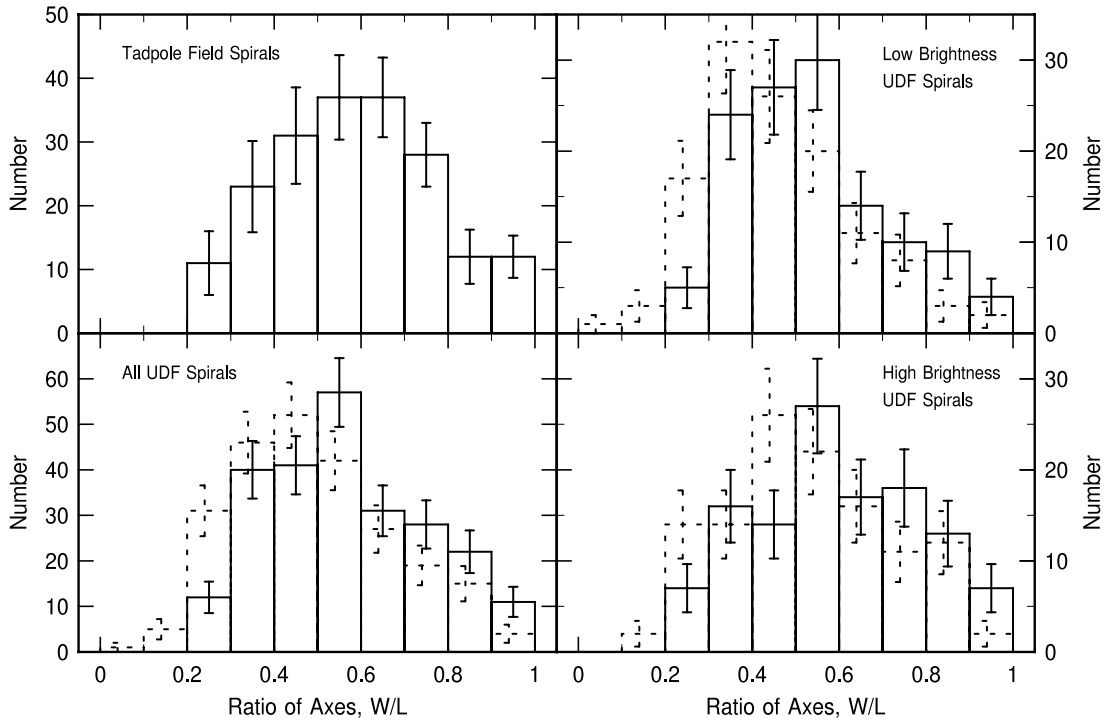

FIG. 8.—Distribution of the ratio of axis (width to length, W/L) for spiral galaxies in the deep field of the Tadpole Galaxy and in the UDF field. The distributions differ significantly from the local distributions (Fig. 9) because of a lack of face-on spirals at high redshift. Randomly oriented disks would have a flat distribution in a diagram like this. The falloff at low W/L results from the intrinsic disk thickness. The position of this falloff is significantly larger at high redshift than for local galaxies, indicating that the high-redshift galaxies have thicker disks.

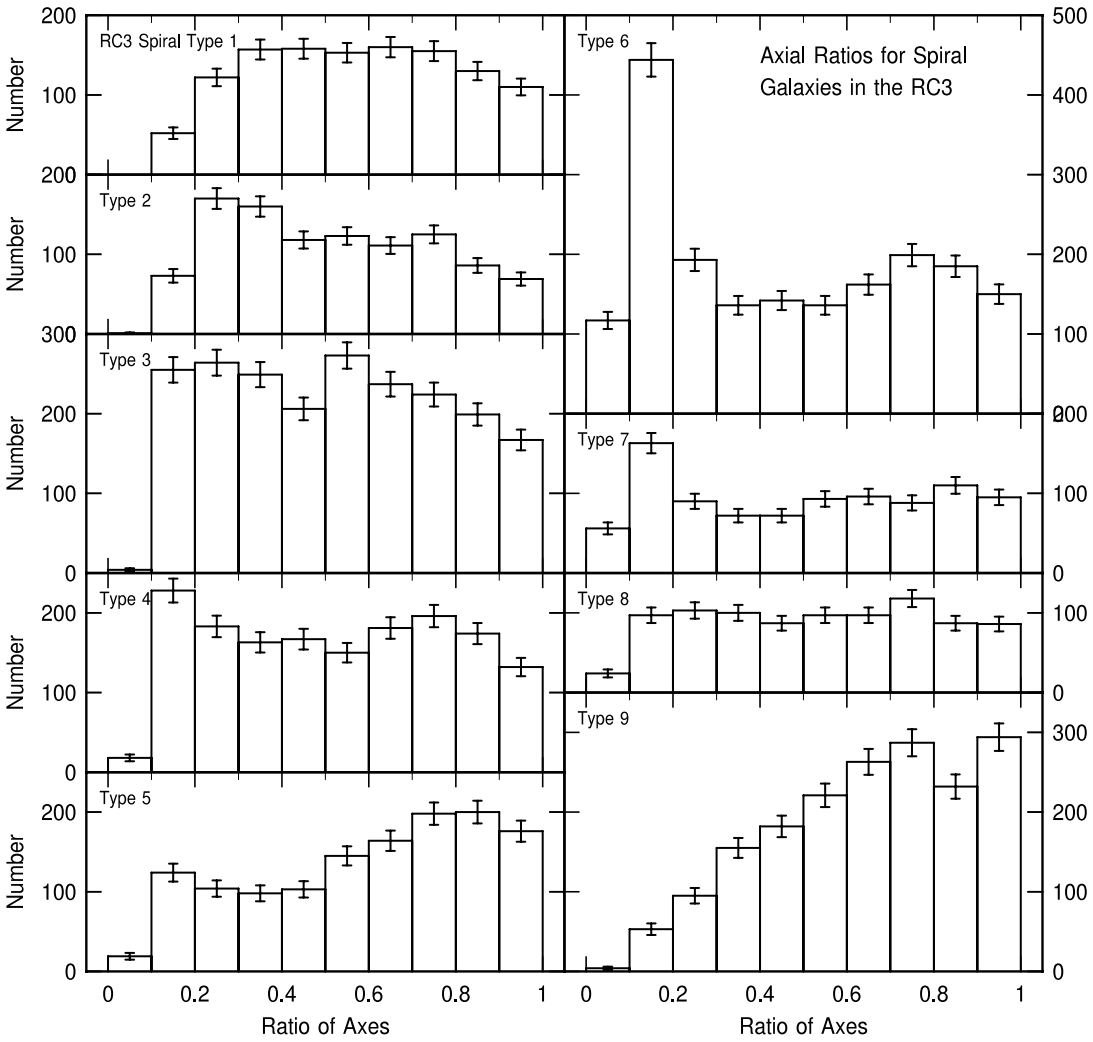

FIG. 9.—Distribution of the ratio of axis for spiral galaxies in the RC3, divided according to de Vaucouleurs type.

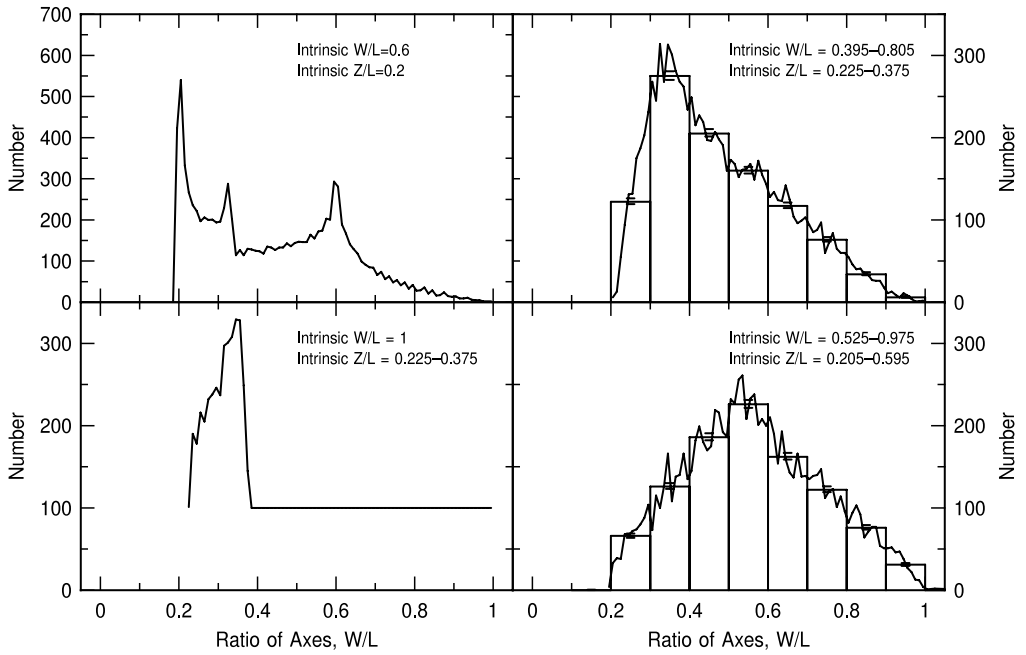

FIG. 10.—Models of distribution of axial ratio for intrinsically triaxial galaxies viewed at random angles, demonstrating how the observed deviations from a uniform distribution could arise at high redshift without surface brightness selection effects. The range of intrinsic width to length (W/L) and thickness to length (Z/L) is indicated on each panel. The two distributions on the right illustrate how the centrally peaked and skewed distributions of the observed spirals can be matched by a triaxial model.

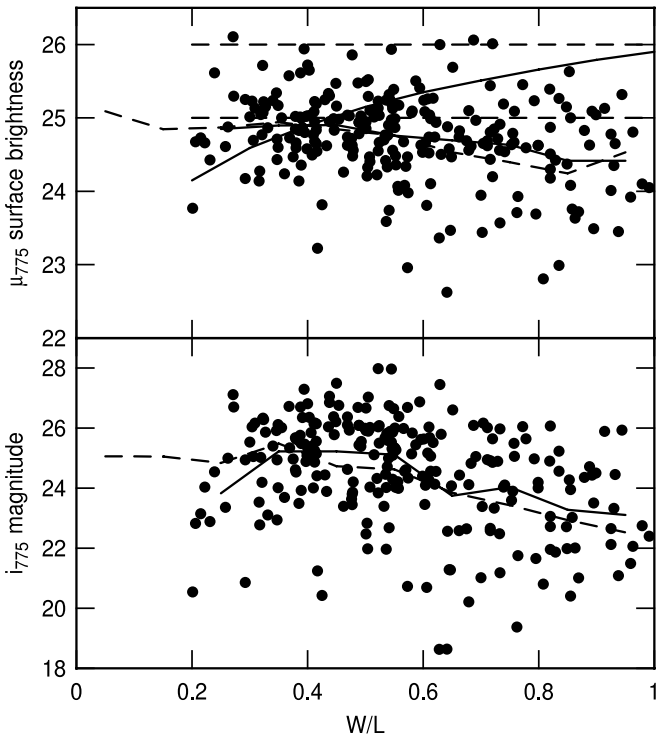

FIG. 11.—Distribution of magnitude and surface brightness for all of the spiral galaxies in this catalog, plotted vs. the apparent ratio of axes, *W/L*. The plotted points and the solid red lines use the axial ratios tabulated in the on-line UDF catalog, while the dashed red lines use the ratio of axes determined by the authors from individual ellipse fits on IRAF. In the bottom panel, the edge-on galaxies are fainter as a result of their lower projected areas. In the top panel, the dashed green lines represent the range of surface brightnesses where galaxies begin to drop below the detection limit. The solid green line is a model where the surface brightness is proportional to the path length through the disk. As the path length decreases for more face-on systems and the average surface brightness becomes fainter, the detection limit is passed and the galaxies disappear from view, making the density of plotted points lower. [*See the electronic edition of the Journal for a color version of this figure.*]

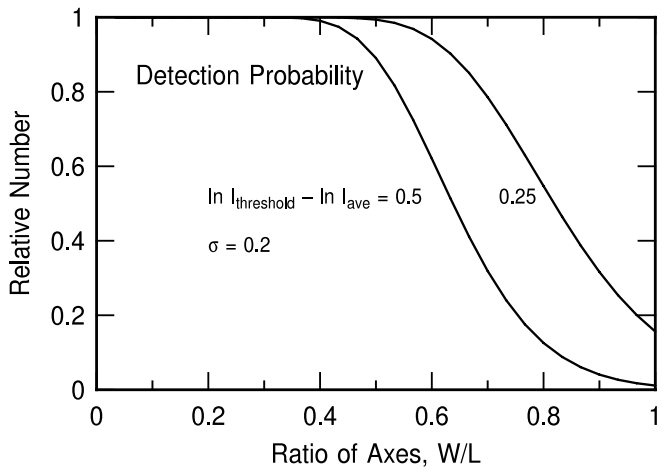

FIG. 12.—Model of the detection probability of spirals that have a distribution of face-on surface brightnesses that is Gaussian in magnitude (i.e., lognormal in intensity) with a dimensionless dispersion $\sigma = 0.2$ and a value at the peak, I_{ave}, fainter than the survey threshold, I_{thresh}, by factors of $e^{0.5}$ and $e^{0.25}$. These two cases bracket the observed falloff in galaxy counts for the range of *W/L* between 0.5 and 1 (as in Fig. 8).

number of galaxies detected above some minimum intensity level. The absolute value of the intensity at the peak of the Gaussian is arbitrary so we take it to be $I_f(\text{peak}) = 1$, and we take the Gaussian dispersion to be σ. The observed intensity of a galaxy with face-on intensity I_f is assumed to be $I_f L/W$, which is approximately the case without extinction (for *W/L* not too small). This means that if an observed intensity is *I*, then the intrinsic face-on intensity for use in the distribution function is *IW/L*. Thus we plot the detection probability:

$$P_{\text{detect}} = \frac{\int_{\ln I_{\text{thresh}}}^{\infty} \exp\left\{-0.5[\ln(IW/L)/\sigma]^2\right\} d\ln I}{\int_{-\infty}^{\infty} \exp\left\{-0.5[\ln(IW/L)/\sigma]^2\right\} d\ln I}. \quad (1)$$

The intensity threshold I_{thresh} and intrinsic dispersion were chosen to match the observed falloff in the distribution of axial ratios between $W/L = 0.5$ and 1. This gives $\ln I_{\text{thresh}}$ between 0.25 and 0.5, or I_{thresh} between $e^{0.25} = 1.3$ and $e^{0.5} = 1.6$ times the intensity at the peak of the lognormal distribution for the two cases plotted. The fit also gives $\sigma = 0.2$.

The fits in Figure 12 indicate that the falloff in spiral galaxy counts between $W/L = 0.5$ and 1 corresponds to a most-probable face-on galaxy surface brightness that is fainter than the threshold of detection by a factor between 1.3 and 1.6. Thus a high fraction of face-on spiral galaxies are likely to be missed and a high fraction of inclined spiral galaxies are likely to be seen (if they satisfy our >10 pixel size selection).

The falloff in galaxy count for face-on spirals does not appear for local galaxies (Fig. 9). This is because there is a limited range in surface brightness for most spiral galaxies and the imaging surveys that made the RC3 went considerably deeper than the average galaxy surface brightness. The fact that there is also not a large increase in local counts at small *W/L* indicates that there is not a relatively large number of thin, ultra–low surface brightness galaxies in the local universe. The situation is apparently different in the UDF because even though galaxies tend to be intrinsically more intense than they are locally, i.e., because of their higher star formation rates, cosmological surface brightness dimming, which is proportional to $(1 + z)^4$, knocks down their apparent surface brightnesses by large factors, corresponding to 3, 4.8, 6, and 7 mag arcsec^{-2} for $z = 1$, 2, 3 and 4. Thus only the brightest of the local galaxies, viewed at these redshifts, would be detected in the UDF survey, and most would be lost unless they were viewed nearly edge-on.

The distribution of axial ratios for chain and clump cluster galaxies in the UDF was shown in Paper III. It is flatter than the spiral galaxy distribution, perhaps because the clumps in clump clusters are very bright and they can still be seen in the face-on versions even if the interclump medium is close to or below the survey limit.

Figure 6 showed a large difference in the apparent magnitude distribution for spirals compared to the linear systems (chains, doubles, and tadpoles) and a modest difference compared to clump clusters, which may be face-on versions of chains. The linear systems dominate at the faintest magnitudes, and some of the reason for this may be the surface brightness selection effects just described, especially since the spiral sample in Figure 6 contains the full range of axial ratios. However, not all of the difference in these distributions is likely to result from surface brightness selection. Paper I showed that even the edge-on spirals in the Tadpole field, as identified by their bulges and exponential disks, tend to have brighter apparent magnitudes and slightly brighter surface brightnesses than the chains, doubles, and tadpoles. This is true also for the edge-on spirals in the UDF sample (not shown here). This difference among the purely edge-on systems could

be the result of a smaller average redshift for the spirals than for the chains, doubles, and tadpoles, which would be consistent with evolution over time from irregular structures to smooth spiral disks. For example, we noted in Paper I that the spirals in the Tadpole field tend to have slightly larger angular sizes than the doubles and tadpoles (by 50% on average). The redshift distributions of galaxies with various morphologies will have to be studied in order to determine the relative importance of surface brightness selection and evolutionary effects.

6. LYMAN BREAK GALAXIES

Steidel et al. (1999 and references therein) identified high-z galaxies photometrically by their redshifted Lyman break. Adelberger et al. (2004) and others applied the technique to galaxies between redshifts 1 and 3. In the UDF field, Lyman break galaxies (LBGs) appear as B-band dropouts at $z \sim 4$ and V-band dropouts at $z \sim 5$. Giavalisco et al. (2004) gave color criteria for LBGs, based on a sample of LBGs in the GOODS/ACS survey. Based on their criteria, we find in our UDF sample 30 B-band dropouts (10 chains, 4 clump clusters, 8 doubles, 4 tadpoles, 1 spiral, and 3 ellipticals) and 13 V-band dropouts (1 chain, 3 clump clusters, 8 doubles, and 1 tadpole). These galaxies are identified by their type and UDF catalog number in Table 7. In Figure 5 many of the objects redder than $\sim$1.5 in $B_{435} - V_{606}$ are B-band dropouts. There are many other LBG galaxies in the UDF that are smaller than our 10 pixel major axis limit (Bouwens et al. 2004). Bunker et al. (2004) and Yan & Windhorst (2004) reported over 100 i-band dropout ($z \sim 6$) galaxies in the UDF; one of our V-band dropout chain galaxies was also reported at redshift $z = 5.4$ by Rhoads et al. (2004).

Most of the dropouts in Table 7 are linear galaxies (doubles, chains, tadpoles) and relatively few are disks (spirals). This is consistent with the common perception that disks form late, but it may also contain a selection bias like that discussed in the previous section if most face-on disks are fainter than the survey limit.

Madau et al. (1998) determined star formation rates (SFRs) from models of star clusters with Salpeter initial mass functions based on observed UV fluxes. Using their conversions, and assuming that the rest wavelength of 1500 Å is shifted approximately to i_{775} band for the $z \sim 4$ galaxies and to z_{850} band for $z = 5$, we calculated the SFRs (in $M_\odot$ yr^{-1}) of our LBGs. The results are listed in Table 7. The SFRs for the V-band dropouts in this sample tend to be larger than for the B-band dropouts. In comparison, Immeli et al. (2004) predicted an SFR of about 20 $M_\odot$ yr^{-1} from their chain-galaxy models, which assumed galaxy sizes a factor of 5 larger than those of our LBGs. Somerville et al. (2001) got rates of $\sim$1–30 $M_\odot$ yr^{-1} for the largest galaxies considered in their Lyman break models.

7. SUMMARY

We classified and measured 884 galaxies larger than 10 pixels in the Hubble UDF. Six prominent types were used: chain, clump cluster, double, tadpole, spiral, and elliptical. Their colors, magnitudes, and surface brightnesses are similar, reflecting their likely formation over a large range of times. The distribution of axial ratios for elliptical galaxies is similar to that in the local field, suggesting that the elliptical shapes were quickly established and remained unchanged over time. The distribution of axial ratios for spiral galaxies was distinctly different than for local galaxies with a deficit of face-on spirals in the deep field. Models illustrate how this could be the result of an intrinsically oval shape, as might be expected for highly perturbed galaxies. However, other models suggest that most of the face-on spirals could be lost below the surface brightness limit of the survey, while the more highly inclined spirals could still be seen. A significant lack of spiral galaxies with low axial ratios implies an intrinsic disk thickness of 0.2 to 0.3 times the disk length. This implies the spiral disks are thicker than local spirals by a factor of $\sim$2–3.

Twenty-six barred spiral galaxies were found, a fraction of the total spirals equal to about 10%. This is a factor of 2 less than other deep field studies but not inconsistent with them considering projection effects and surface brightness dimming. In addition, bars become harder to distinguish at high redshifts because the spiral galaxies generally become more irregular.

We thank the Vassar College URSI program and the Keck Northeast Astronomy Consortium exchange program for undergraduate research support for M. S. and D. S. R.; B. G. E. is supported by the National Science Foundation through grant AST 02-05097.

REFERENCES

Abraham, R., Tanvir, N., Santiago, B., Ellis, R., Glazebrook, K., & van den Bergh, S. 1996a, MNRAS, 279, L47
Abraham, R., van den Bergh, S., Glazebrook, K., Ellis, R., Santiago, B., Surma, P., & Griffiths, R. 1996b, ApJS, 107, 1
Adelberger, K., Steidel, C., Shapley, A., Hunt, M., Erb, D., Reddy, N., & Pettini, M. 2004, ApJ, 607, 226
Athanassoula, E., & Bosma, A. 2003, Ap&SS, 284, 491
Binggeli, B., & Popescu, C. C. 1995, A&A, 298, 63
Bouwens, R. J., Illingworth, G. D., Blakeslee, J. P., Broadhurst, T. J., & Franx, M. 2004, ApJ, 611, L1
Brinchmann, J., et al. 1998, ApJ, 499, 112
Bruzual, G., & Charlot, S. 2003, MNRAS, 344, 1000
Bunker, A., Stanway, E., Ellis, R., & McMahon, R. 2004, MNRAS, 355, 374
Conselice, C. 2005, in Multiwavelength Mapping of Galaxy Formation and Evolution, ed. R. Bender & A. Renzini (Berlin: Springer), in press (astro-ph/0405102)
Conselice, C., et al. 2004, ApJ, 600, L139
Cowie, L., Hu, E., & Songaila, A. 1995, AJ, 110, 1576
Dalcanton, J. J., & Schectman, S. A. 1996, ApJ, 465, L9
de Vaucouleurs, G., de Vaucouleurs, A., Corwin, H. G., Jr., Buta, R. J., Paturel, G., & Fouqué, P. 1991, Third Reference Catalogue of Bright Galaxies (New York: Springer)
Dickinson, M. 2000, Philos. Trans. R. Soc. London, A, 358, 2001
Elmegreen, B. G., & Elmegreen, D. M. 2005, ApJ, 627, 632 (Paper III)
Elmegreen, D. M., Elmegreen, B. G., & Ferguson, T. E. 2005, ApJ, 623, L71 (Paper IV)
Elmegreen, D. M., Elmegreen, B. G., & Hirst, A. C. 2004a, ApJ, 604, L21 (Paper II)
———. 2004b, ApJ, 612, 191 (Paper V)
Elmegreen, D. M., Elmegreen, B. G., & Sheets, C. M. 2004c, ApJ, 603, 74 (Paper I)
Ferguson, H. C., Dickinson, M., & Williams, R. 2000, ARA&A, 38, 667
Franceschini, A., Silva, L., Fasano, G., Granato, G. L., Bressan, A., Arnouts, S., & Danese, L. 1998, ApJ, 506, 600
Freeman, K. C. 1970, ApJ, 160, 811
Giavalisco, M., et al. 2004, ApJ, 600, L103
Immeli, A., Samland, M., Westera, P., & Gerhard, O. 2004, ApJ, 611, 20
Jogee, S., et al. 2004, ApJ, 615, L105
Madau, P., Pozzetti, L., & Dickinson, M. 1998, ApJ, 498, 106
Merritt, D., & Tremblay, B. 1996, AJ, 111, 2243
O'Neil, K., Bothun, G. D., & Impey, C. D. 2000, ApJS, 128, 99
Reshetnikov, V., Battaner, E., Combes, F., & Jiménez-Vicente, J. 2002, A&A, 382, 513
Reshetnikov, V., Dettmar, R.-J., & Combes, F. 2003, A&A, 399, 879
Rhoads, J., et al. 2005, ApJ, 621, 582
Sheth, K., Regan, M. W., Scoville, N. Z., & Strubbe, L. E. 2003, ApJ, 592, L13
Somerville, R. S., Primack, J. R., & Faber, S. M. 2001, MNRAS, 320, 504

Steidel, C., Adelberger, K., Giavalisco, M., Dickinson, M., & Pettini, M. 1999, ApJ, 519, 1
Straughn, A., Ryan, E., Cohen, S., Hathi, N., Windhorst, R., & Pasquali, A. 2004, BAAS, 205, 9417
Sung, E.-C., Han, C., Ryden, B. S., Patterson, R. J., Chun, M.-S., Kim, H.-I., Lee, W.-B., & Kim, D.-J. 1998, ApJ, 505, 199
Thompson, R., et al. 2005, AJ, 130, 1
Tran, H., et al. 2003, ApJ, 585, 750
Tully, R. B., & Fisher, J. R. 1977, A&A, 54, 661
van den Bergh, S. 2002, PASP, 114, 797
van den Bergh, S., Abraham, R. G., Ellis, R. S., Tanvir, N. R., Santiago, B. X., & Glazebrook, K. G. 1996, AJ, 112, 359
van den Bergh, S., Abraham, R. G., Whyte, L. F., Merrifield, M. R., Eskridge, P. B., Frogel, J. A., & Pogge, R. 2002, AJ, 123, 2913
van den Bergh, S., Cohen, J. G., Hogg, D. W., & Blandford, R. 2000, AJ, 120, 2190
Volonteri, M., Saracco, P., & Chincarini, G. 2000, A&AS, 145, 111
Williams, R., et al. 1996, AJ, 112, 1335
Yan, H., & Windhorst, R. A. 2004, ApJ, 612, L93